Electronic Supplementary Information: Rearrangement of Van-der-Waals Stacking and Formation of a Singlet State at T = 90 K in a Cluster Magnet

John P. Sheckelton,[a,b] Kemp W. Plumb,[b] Benjamin A. Trump,[a,b] Collin L. Broholm,[b,c,d] and Tyrel M. McQueen[a,b,c,*]

1 Synchrotron powder diffraction analysis

Table 1 is a summary of Rietveld refinement parameters to T = 300 K synchrotron X-ray powder diffraction data shown in main text Fig. 1(a). Low temperature synchrotron X-ray powder diffraction data near liquid nitrogen temperatures shows no signs of symmetry lowering distortions despite a temperature reading of approximately 80 K near the sample. Rietveld refinement of the HT ($P\bar{3}m1$) structure to the data near liquid nitrogen temperatures is shown in Fig. S1 and is summarized in Table 2. 80 K is far below the first-order phase transition in Nb_3Cl_8 ($\approx$ 90 K)—the absence of any Nb_3Cl_8 LT phase, therefore, is attributed to sample heating from the 30 KeV ($\lambda \approx 0.41$ Å) incident X-ray beam. As is the case with the T = 300 K data, fitting the low temperature data to lower symmetry models ($P\bar{3}$, $P3m$, $P3$, and $C2/m$) results in no improvement of the fit, either quantitatively or qualitatively.

Table 1: Nb_3Cl_8 Rietveld refinement to synchrotron X-ray ($\lambda = 0.4132$ Å) powder diffraction data at T = 300 K, shown in main text Fig. 1(a). The spacegroup is $P\bar{3}m1$ (164) with lattice parameters $a = 6.74566(3)$ Å, $c = 12.28056(7)$ Å, $\alpha = \beta = 90^o$, and $\gamma = 120^o$. All sites are fully occupied, cell volume was calculated to be $V = 483.947(6)$ Å^3, and atomic displacement parameters were freely refined for all atoms. The fit quality is given by $R_{wp} = 11.34\,\%$, $R_p = 9.03\,\%$, and $\chi^2 = 3.286$. Errors are computed statistical uncertainties.

Atom	Wyckoff position	x	y	z	U_{iso}(Å^2)
Nb	6*i*	0.52763(2)	0.05525(5)	0.24577(5)	0.00473(6)
Cl-1	2*d*	2/3	1/3	0.0978(2)	0.0045(4)
Cl-2	2*d*	1/3	2/3	0.3555(2)	0.0085(5)
Cl-3	6*i*	0.6696(2)	-0.1652(1)	0.1350(1)	0.0069(3)
Cl-4	6*i*	0.3374(2)	0.1687(1)	0.3835(1)	0.0103(3)

Table 2: Nb_3Cl_8 Rietveld refinement to synchrotron X-ray ($\lambda = 0.4132$ Å) powder diffraction data at $T \approx 90$ K, shown in Fig. S1. The spacegroup is $P\bar{3}m1$ (164) with lattice parameters $a = 6.73255(2)$ Å, $c = 12.22222(5)$ Å, $\alpha = \beta = 90^o$, and $\gamma = 120^o$. All sites are fully occupied, cell volume was calculated to be $V = 479.777(4)$ Å^3, and atomic displacement parameters were freely refined for all atoms. The fit quality is given by $R_{wp} = 9.31\,\%$, $R_p = 7.61\,\%$, and $\chi^2 = 2.141$. Errors are computed statistical uncertainties.

Atom	Wyckoff position	x	y	z	U_{iso}(Å^2)
Nb	6*i*	0.52746(2)	0.05493(4)	0.24622(4)	0.00182(4)
Cl-1	2*d*	2/3	1/3	0.0981(2)	0.0024(3)
Cl-2	2*d*	1/3	2/3	0.3560(1)	0.0041(3)
Cl-3	6*i*	0.6709(1)	-0.16456(6)	0.13528(7)	0.0023(2)
Cl-4	6*i*	0.3359(1)	0.16793(6)	0.38192(8)	0.0051(2)

[a] *Department of Chemistry, The Johns Hopkins University, Baltimore, MD 21218, USA.*
[b] *Institute for Quantum Matter and Department of Physics and Astronomy, The Johns Hopkins University, Baltimore, MD 21218, USA.*
[c] *Department of Materials Science and Engineering, The Johns Hopkins University, Baltimore, Maryland 21218, USA.*
[d] *NIST Center for Neutron Research, National Institute of Standards and Technology, Gaithersberg, MD 20899, USA.*
[*] E-mail: *mcqueen@jhu.edu*

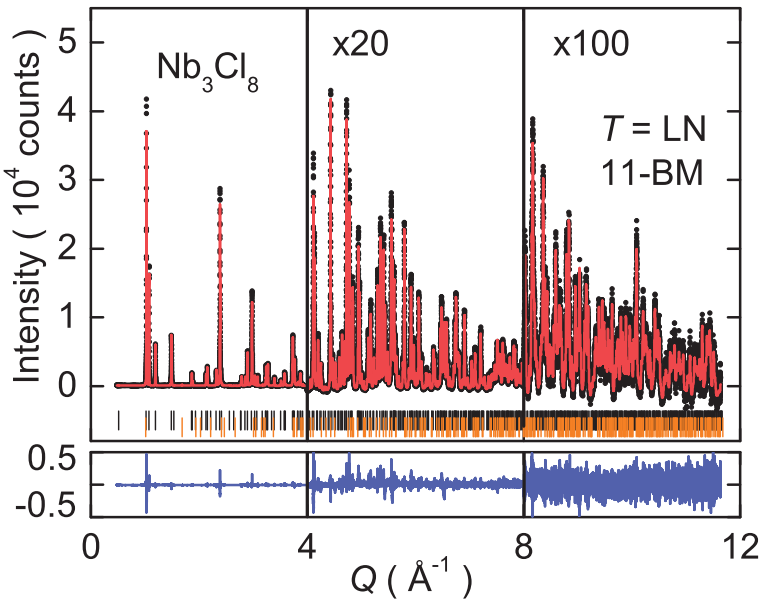

Figure S1: Nb_3Cl_8 Rietveld analysis of synchrotron X-ray diffraction data at liquid nitrogen (LN) temperatures. Black dots are data, red line is the calculated fit, blue line is the difference, tick marks are Bragg reflections for Nb_3Cl_8 (black) and a minor impurity, $NbOCl_2$ (orange, 0.5(2) wt%). The higher Q data are multiplied $\times 20$ ($4 \geq Q \geq 8$) and $\times 100$ ($8 \geq Q \geq 12$) to highlight the quality of the fit.

2 DFT band structure calculations

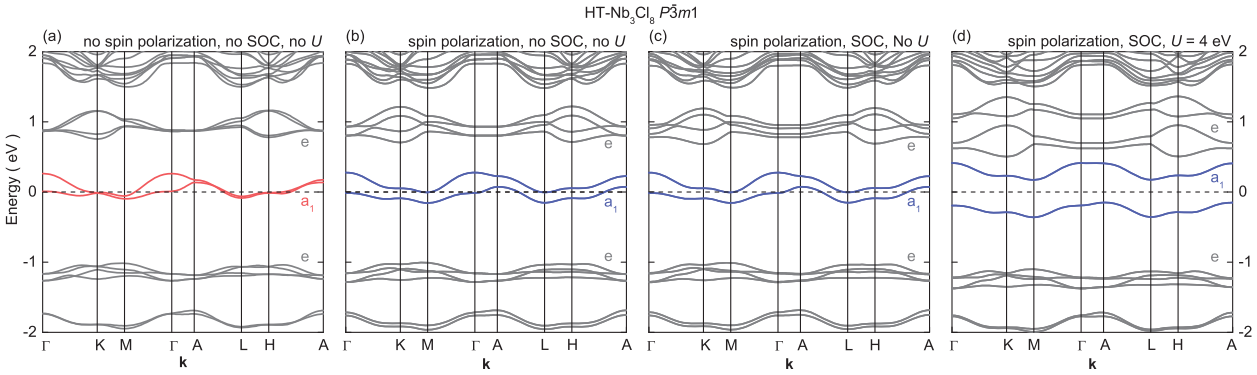

Figure S2: Band structure calculations on HT-Nb_3Cl_8 with (a) no spin polarization (SP), spin-orbit coupling (SOC), or Hubbard U, (b) SP but no SOC/U (c) SP and SOC but no U, and (d) SP, SOC, and $U = 4$ eV. The red highlighted bands in (a) are the highest occupied a_1 orbitals, which are split at the Γ-point from the formation of a bonding/anti-bonding pair and are far in energy (≈ 1 eV) from the degenerate e orbitals. In (b)-(d), the total splitting of the a_1 band (blue) is due to antiferromagnetic order. The spin polarized calculations are initiated with the application of an applied field to break spin degeneracy. This results in calculations (b)-(d) converging with antiferromagnetic order where Nb_3Cl_{13} cluster spins are oriented in the crystallographic c-axis. In (d), the antiferromagnetic band splitting is exacerbated by the electronic interaction induced by the Hubbard U.

Calculations on the high temperature (HT) structure of Nb_3Cl_8 were performed without spin-polarization [Fig. S2 (a)], with spin-polarization [Fig. S2 (b)], with spin-orbit coupling [Fig. S2 (c)], and with a Hubbard U term [Fig. S2 (d)], all of which display the same qualitative highest occupied molecular orbital (HOMO) splitting at the Γ point as in Fig. S2 (a). The calculations in Fig. S2 (b)-(d) have an additional splitting of the HOMO bands over the entire Brillouin zone originating from the formation of antiferromagnetic order between ferromagnetic planes. The onset of antiferromagnetic order in Fig. S2 (b)-(d) stems from the initial application of a magnetic field to split spin degeneracy despite a reduction of the applied field with subsequent calculation iterations and a convergence with no applied field. The application of a Hubbard U, Fig. S2 (d), is required to fully open the gap and predict insulating behavior. The splitting observed in the a_1 derived bands in these calculations is allowed due to the unit cell symmetry and there being an

even number of electrons per unit cell [1]. The large cluster interaction energy indicated by the width of the a_1 band (≈ 200 meV) clearly plays a key role in the collective transition from a triangular lattice $S = 1/2$ antiferromagnet to a system of static singlets.

The special points of the Brillouin zone used in the HT phase calculations are for a trigonal unit cell in the hexagonal setting and are $\Gamma = (000)$, $K = (\frac{1}{3}\frac{2}{3}0)$, $M = (0\frac{1}{2}0)$, $A = (00\frac{1}{2})$, $L = (0\frac{1}{2}\frac{1}{2})$, and $H = (\frac{1}{3}\frac{2}{3}\frac{1}{2})$. The special points of the Brillouin zone for a monoclinic unit cell in the $C2/m$ space group with unique axis b, cell choice 1 used in the LT calculations are $V = (\frac{1}{2}00)$ $Z = (\frac{1}{2}\frac{1}{2}0)$ $\Gamma = (000)$ $A = (00\frac{1}{2})$ $M = (\frac{1}{2}\frac{1}{2}\frac{1}{2})$ $L = (\frac{1}{2}0\frac{1}{2})$.

3 Spin-Peierls analysis

The transition into a spin-Peierls (SP) state is marked by an exponential decay of the magnetic susceptibility as a function of temperature [2]. The SP transition temperature depends on the magnetic interaction strength and the spin excitation gap in the SP state. Nb_3Cl_8 does not have an exponential decay into the low-temperature (LT) state—the first-order nature of the transition results in remnant domains of the HT phase upon cooling. Instead, a plot of magnetic susceptibility collected upon warming, Fig. S3, of the $c \parallel \mu_o H$ data [reproduced from main text Fig. 2 (a)] must be used in modeling the behavior of the bulk LT state. As can be seen in Fig. S3, the susceptibility data is flat in temperature (with the exception of the Curie tail in $T \leq 50$ K) up to the transition at $T \approx 100$ K. To test that the magnetic susceptibility from a SP state (χ_{SP}) is varying minimally with temperature, a Curie-Weiss fit to the LT data up to $T = 50$ K and $T = 100$ K was performed to extract a value of $\chi_o \approx \chi_{SP}$ for the two temperature regions, a deconvolution of the Curie tail contribution. Values of $\chi_o = 0.8$ and 0.7×10^{-4} emu $\cdot$ Oe^{-1} $\cdot$ mol $f.u.^{-1}$ are extracted for fits up to $T = 100$ K and $T = 50$ K respectively.

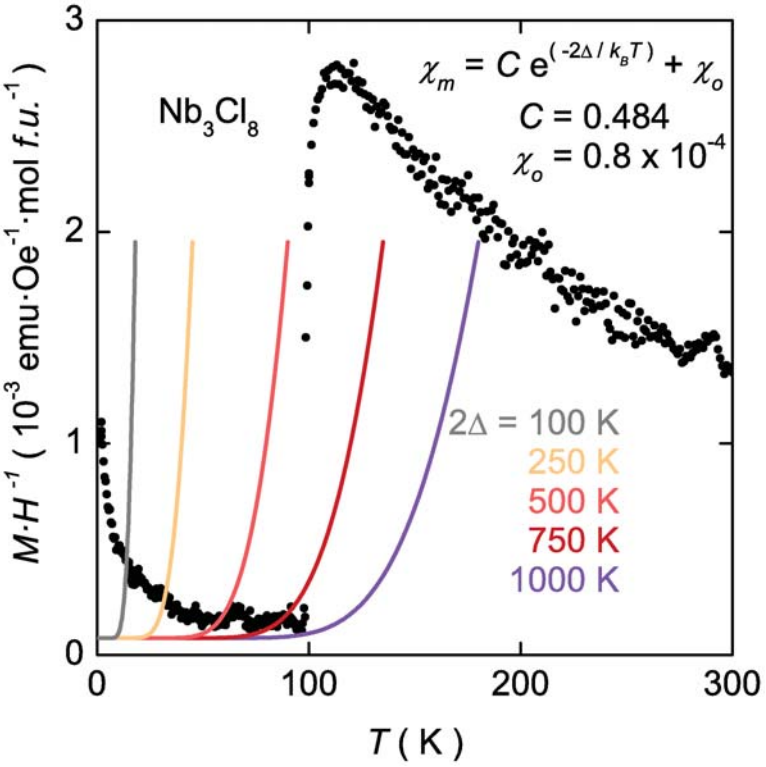

Figure S3: Nb_3Cl_8 magnetic susceptibility data (black dots) as a function of temperature upon warming. The data at LT is a convolution of a Curie tail and the intrinsic behavior of the LT magnetic state of Nb_3Cl_8. The colored lines are calculations of the exponential behavior expected of a spin-Peierls state. As can be seen, a gap of at least $2\Delta = 1000$ K must exist in order to observe the magnetic behavior of a spin-Peierls state in Nb_3Cl_8.

The magnetic behavior of a SP state can be approximated by the exponential [3]

$$\chi_m = C\, e^{\frac{-2\Delta}{k_B T}} + \chi_o$$

where χ_m is the molar susceptibility, C is the Curie constant, 2Δ is the gap to the first excited state, k_B is Boltzmann's constant, and χ_o is the temperature independent contribution to the susceptibility. It is important to note that the

transition temperature between HT and LT states in Nb_3Cl_8 is not necessarily the spin-Peierls transition—since the transition in Nb_3Cl_8 is first-order, the HT and LT magnetic behaviors need not be related in any way. Assuming the LT state in Nb_3Cl_8 is a SP state, then calculations for various magnitudes of the spin gap show that the gap must be at least $2\Delta = 1000\,\mathrm{K}$ in order reproduce the observed behavior. These calculations assume the Curie constant is the value extracted from the HT fit for a S = 1/2 system, $C = 0.484\ \mathrm{emu \cdot K \cdot mol}\, f.u.^{-1} \cdot \mathrm{Oe}^{-1}$, and the temperature independent contribution is $\chi_o = 0.8 \times 10^{-4}\ \mathrm{emu \cdot Oe^{-1} \cdot mol}\ f.u.^{-1}$.

The magnitude of the spin gap may also be estimated, assuming LT Nb_3Cl_8 is a spin-Peierls state and the transition temperature $T_c = 100\,\mathrm{K}$, by examining the ratio of the susceptibility above and below the transition as is done in other SP materials such as $CuGeO_3$ [4]. Approximating $\chi_{HT}/\chi_{LT} \approx R$, and rearranging $R = e^{\frac{-\Delta}{T_c}}$ to $\Delta = T_c \cdot ln(R)$ with $R \approx 30$ gives $\Delta = 100\,\mathrm{K} \cdot ln(30) = 340\,\mathrm{K}$. This is on the same order as to what may be expected of a SP system, where the gap $\Delta \approx 1.5 \cdot T_c$.

We can also make an approximation of the exchange constant J in the Nb_3Cl_8 spin-Peierls system from the spin-phonon coupling constant given by Cross and Fisher [5]. Here, $T_c = 0.8 \cdot J \cdot \eta$, or $J = \frac{T_c \cdot 1.25}{\eta}$. Assuming the value of η used for $CuGeO_3$, $\eta = 0.2$, is used for Nb_3Cl_8, the calculation yields a $J = \frac{100\,\mathrm{K} \cdot 1.25}{0.2} = 625\,\mathrm{K}$— much larger than the value extracted from the Curie-Weiss fit to the HT susceptibility data of $\theta = 51.2\,\mathrm{K}$. This discrepancy may be indicative of a strong enhancement of the exchange constants upon entering the LT state from the structural rearrangement, or that a spin-Peierls model fails to adequately explain the magnetic behavior of Nb_3Cl_8.

References

[1] James M. Rondinelli and Nicola A. Spaldin. Structure and Properties of Functional Oxide Thin Films: Insights From Electronic-Structure Calculations. *Advanced Materials*, 23(30):3363–3381, August 2011.

[2] L. N. Bulaevskii, A. I. Buzdin, and D. I. Khomskii. Spin-peierls transition in magnetic field. *Solid State Communications*, 27(1):5–10, July 1978.

[3] P. J. Baker, S. J. Blundell, F. L. Pratt, T. Lancaster, M. L. Brooks, W. Hayes, M. Isobe, Y. Ueda, M. Hoinkis, M. Sing, M. Klemm, S. Horn, and R. Claessen. Muon-spin relaxation measurements on the dimerized spin-12 chains $NaTiSi_2O_6$ and TiOCl. *Physical Review B*, 75(9):094404, March 2007.

[4] Masashi Hase, Ichiro Terasaki, and Kunimitsu Uchinokura. Observation of the spin-Peierls transition in linear Cu^{2+} (spin-1/2) chains in an inorganic compound $CuGeO_3$. *Physical Review Letters*, 70(23):3651–3654, June 1993.

[5] M. C. Cross and Daniel S. Fisher. A new theory of the spin-Peierls transition with special relevance to the experiments on TTFCuBDT. *Physical Review B*, 19(1):402–419, January 1979.